THE PENNSYLVANIA STATE UNIVERSITY
SCHREYER HONORS COLLEGE

DEPARTMENT OF ELECTRICAL ENGINEERING

THE DESIGN AND TESTING OF A ROCKET-BORNE NOCTILUCENT CLOUD PHOTOMETER

MICHAEL A. ORATIS

Fall 2005

A thesis
submitted in partial fulfillment
of the requirements
for a baccalaureate degree
in Electrical Engineering
with honors in Electrical Engineering

Approved: _____ Date: _____
C. Russell Philbrick
Thesis Supervisor

_____ _____
John D. Mitchell
Honors Adviser

ABSTRACT

Penn State's rocket-launch program, SPIRIT, brings together an international coalition of students interested in designing experiments and constructing a rocket payload to measure the high-latitude atmosphere. SPIRIT's optics team has particular interest in investigating the properties of noctilucent clouds (NLC) present in the mesosphere. The purpose of studying NLC is that a better understanding of their properties may provide insight into the global atmospheric changes caused by pollutants present in the atmosphere and the global energy balance. The analysis of the solar radiation that the NLC particles scatter will provide insight to the number and size distribution from measurements by a rocket-borne photometer aboard SPIRIT's payload.

This report includes a description of the following topics: NLC, Mie scattering theory, past rocket-borne photometers, photometer circuitry, circuit analysis, photometer layout, and preliminary lab-based design tests.

TABLE OF CONTENTS

LIST OF FIGURES

LIST OF TABLES

1 INTRODUCTION

1.1 NLC INTRODUCTION

At specific locations and specific seasons, one may observe a remarkably beautiful phenomenon present in the upper atmosphere; they may appear visibly faint, or with mysterious-looking, multi-colored wisps. These night-shining clouds are known as noctilucent clouds, or simply NLC. The term "noctilucent" is a Latin derivative, meaning night shining. Their nighttime glimmer is a result of their being so high in the atmosphere, such that they remain in the sunlight long after sunset.

The first recorded observation of noctilucent clouds was in the summer of 1884 from Krakatoa Island, some time after it was destroyed by a volcanic eruption. As such, early theories explain the NLC formation as a result of the eruption; however, current views suggest that the eruption had no direct effect on their formation. The mere beauty and height of the noctilucent clouds are what allowed early observers to easily distinguish them from lack-luster, low-lying clouds [Martin, 2004].

1.2 NLC FORMATION

Noctilucent clouds are present in the mesosphere of the upper-atmosphere, at altitudes of more than 80 km above sea level. At this altitude, the atmosphere is very dry, and the air pressure is a few millionths of that at sea level. As such, water molecules are present at only a few ppm; the available water there for cloud formation is clearly minute. So, in order for the dew point to be sufficiently low for clouds to form at this location, dense enough to scatter enough light to be visible, there must be unusually cold conditions. Such conditions are made possible by global circulation of the upper atmosphere, the

result of solar heating in regions of the atmosphere below the NLC level, which forces upward expansion of air over the summer polar regions, and downward warming of air over the winter polar regions; interestingly, the upper atmosphere is colder in the summer than in the winter.

The first accurate temperature profile through a noctilucent cloud was obtained during the CAMP campaign from ESRANGE Sweden in August 1982 [Philbrick et al, 1984]. A piezoelectric accelerometer measured a temperature of 111° K at the location of a minimum created by the gravity wave structure, and a temperature of 138° K at the NLC layer, lower in altitude.

The primary reason for the cold summer mesopause is due to the cutoff of the primary heat source of the mesopause region. The ALADDIN campaigns during the early 1970's showed that the turbulence created by gravity wave breaking in the mesopause region resulted in heating rates of about 4° K per day during most of the year [Philbrick, 1973 and Zimmerman et al, 1979]. However, during the summer, the zonal wind flow in the lower atmosphere effectively removes the high frequency components of the gravity wave spectrum, thereby reducing this important heat source and resulting in the growth and presence of the low frequency and large amplitude of the longer wavelength features.

At such a low temperature, water molecules gather together to form ice particles. As these water molecules diffuse up through the atmosphere they may photodissociate in the presence of ultraviolet radiation, producing free radicals. Water molecules are lost from the mesosphere through dissociation that produces hydrogen atoms which are

manifest in the exosphere. Water cluster ions can provide a likely precursor to the visible aerosol layers that develop as the noctilucent clouds [Witt et al, 1971].

1.3 NLC OBSERVATION

NLC are generally observed by amateurs. Cloud visibility is limited between one to five nights, during three months out of the year, and thus scientific funding is seldom approved for NLC observation. On those mysterious nights, noctilucent clouds are visible in mid- to upper-latitudes between 55° and 60°N [Gadsden and Schröder 1989]. The NLC are also usually difficult to see because of their high altitude and tenuous nature. Observations are generally very expensive, but a few rocket payloads have been used for measurements of NLC particle characteristics, and these have provided current knowledge about noctilucent clouds.

1.4 NLC TYPES

There are five internationally standard types of Noctilucent clouds:

Type I – Veils, generally a background, lacking definition

Type II – Bands, look like long parallel wisps

Type III – Billows, shorter wisps, also generally parallel

Type IV – Whirls, dark-centered rings

Type V – Amorphous, similar to veils, but tend to be brighter and more visible

[Gadsden and Schröder 1989].

2 MIE SCATTERING

2.1 MIE SCATTERING THEORY

Mie theory, also called Lorenz-Mie theory, is a complete mathematical-physical theory of the scattering of electromagnetic radiation by spherical particles, developed by Gustav Mie in 1908 ["Mie Theory," 2005]. Because NLC particles are so small compared to wavelength, they appear to scatter similar to spheres. For specific wavelengths and particle sizes, a computerized model of Mie theory can draw theoretical scatter plots. Comparing a photometer-generated scatter plot to that theorized by the Mie computer model, conclusions can be drawn about NLC particle size. Notice Figure 2.1.1 below. For a given scattering angle, and a given wavelength of the incident solar radiation, Mie theory can predict the intensity of the resultant scatter. Experimentally, as the rocket spins about its axis, the photometer will collect scattered radiances at all possible scattering angles and an experimental scatter plot can then be drawn.

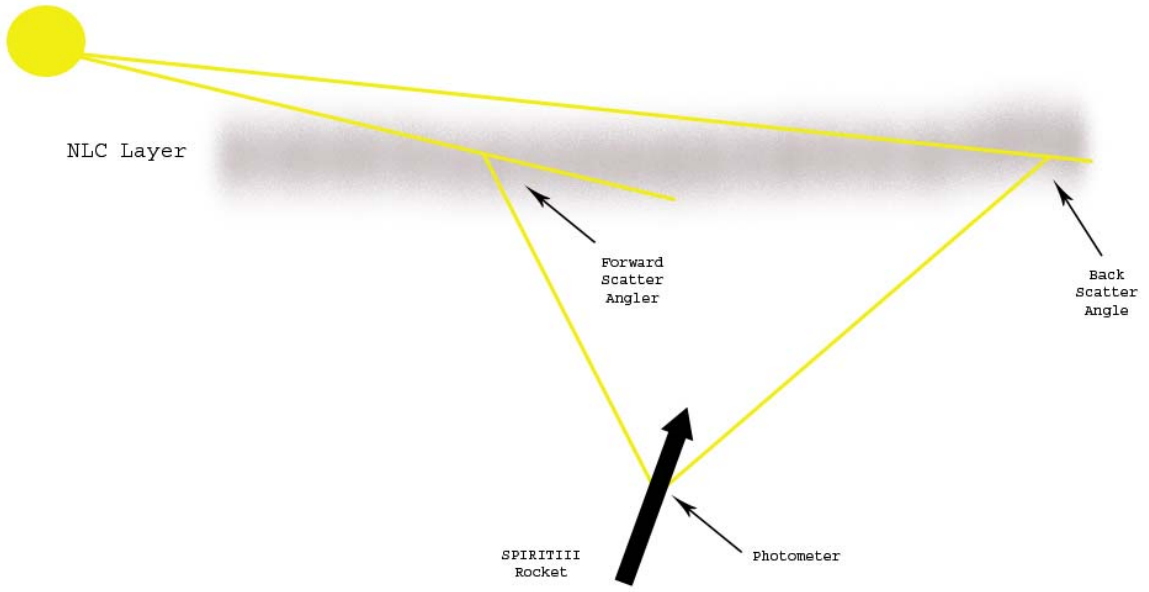

Figure 2.1.1: NLC Solar Radiation Scatter

2.2 MIE SCATTER THEORY PLOTS – A MATLAB EXAMPLE

In order to generate theoretical NLC scatter plots for specific wavelengths and particle sizes, a MATLAB model of Mie scattering will be used. The MATLAB code that is used to generate scatter examples has been provided courtesy of Sachin Verghese from Penn State University. The following assumptions are made:

Index of refraction of surrounding medium:	1 (air)
Index of refraction of cloud particles:	1.33 (water)
Effective wavelength of solar radiation:	550 nm (one of several passband filters to be used)
Particle radius:	0.01 μm

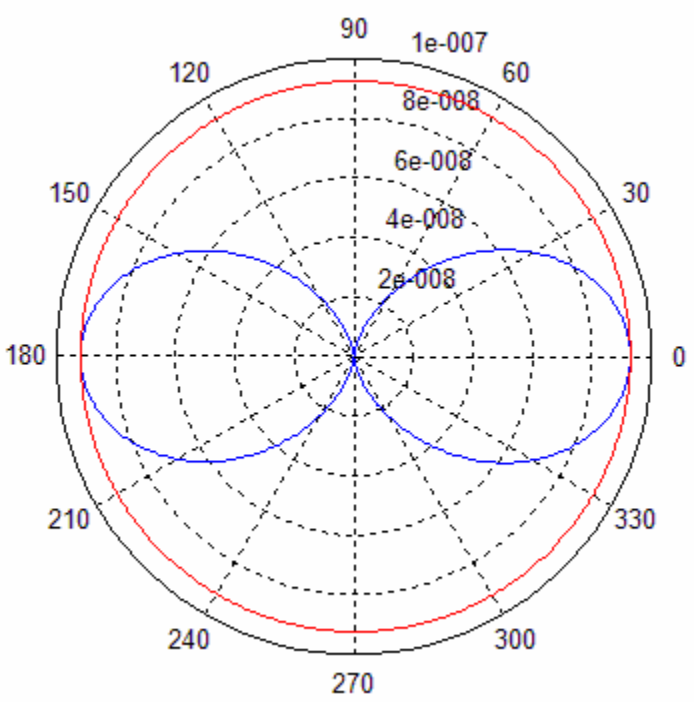

Figure 2.2.1: Theoretical Scatter Plot

Figure 2.2.1 shows the theoretical scatter plot for the previous assumptions. Now, suppose the photometer generated data whose plot showed similar characteristics

throughout the scatter angles, one could assume a particle radius near 0.01 μm. A second example is shown in Figure 2.2.2 with the follow assumptions:

Index of refraction of surrounding medium:	1 (air)
Index of refraction of cloud particles:	1.33 (water)
Effective wavelength of solar radiation:	550 nm (one of several passband filters to be used)
Particle radius:	0.1 μm

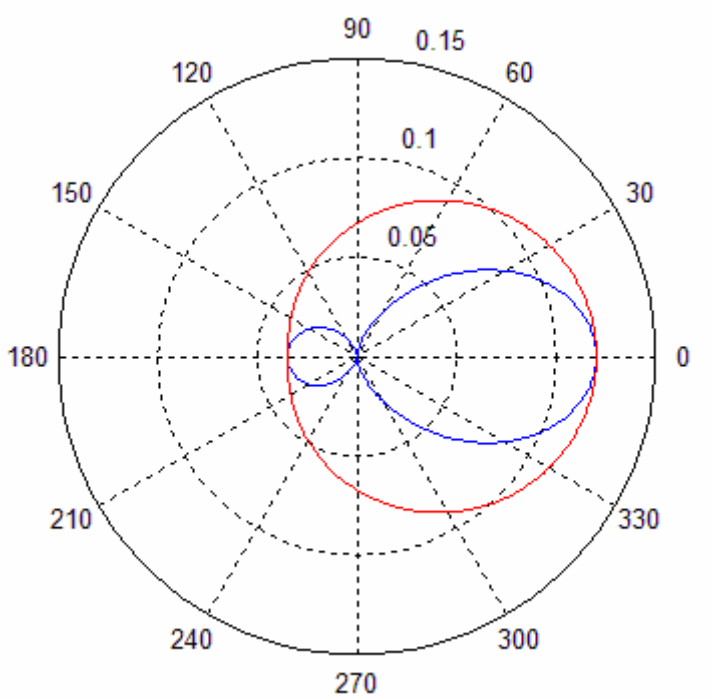

Figure 2.2.2: Theoretical Scatter Plot

Figure 2.2.2 shows a noticeably different scatter plot as the theoretical particle radius was increased. A third example, with an again increased particle radius, is shown in Figure 2.2.3 with assumptions:

Index of refraction of surrounding medium:	1 (air)
Index of refraction of cloud particles:	1.33 (water)
Effective wavelength of solar radiation:	550 nm (one of several passband filters to be used)
Particle radius:	1 μm

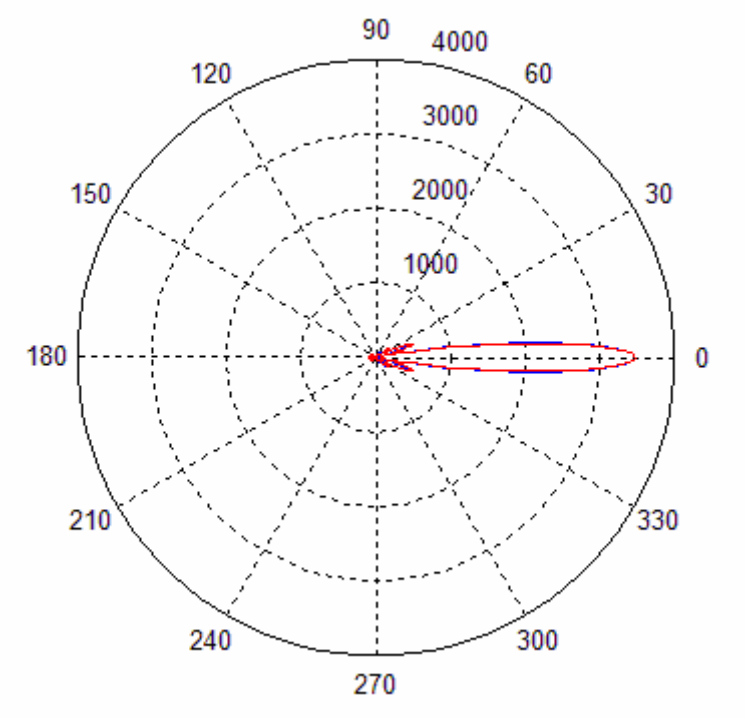

Figure 2.2.3: Theoretical Scatter Plot

Theoretical scatter plots can be drawn for an arbitrary particle radius and effective wavelength of radiation until a match between the theory and experimental data is achieved for particle size conclusion.

2.3 MIE SCATTER THEORY RATIOS

Noticing designs as per Figures 2.2.1-3, there is a large range of data for which the photometer needs to interpret. One way to simplify data interpretation would be to analyze scatter radiation as a ratio of the forward and back scatter. Instead of comparing photometer-driven scatter plots to that theorized by the MATLAB model of Mie theory, forward and back scatter ratios could be used. The MATLAB Mie model would thus be used to generate a ratio for a given pair of angles. For example, notice Figure 2.2.1; a

theoretical forward to back scatter ratio (35° to 145°) would yield approximately unity. Therefore, if the photometer measured near equivalent radiances for 35° and 145°, similarities can be drawn between the theory and the NLC under examination, i.e. a particles radius on the order of 0.01 μm. Comparison of the signals measured over a spin cycle at the same angles when the particle radius is 0.1 μm result in a ratio of about 3.2. By examining the variation over a spin cycle and measuring at several wavelengths, the size distribution and particle density in the noctilucent cloud can be described.

3 DESIGN

3.1 OVERVIEW

As mentioned, there is a large expected range of values for which the photometer must measure. As such, each photometer channel will include two, overlapping scaled voltage outputs to extend the range of data. And, as the photometer needs to measure over a large range of angles, it will include ten photodiode channels aligned two by five (Figure 3.1.1). Each channel will have a five degree viewing angle (Figure 3.1.2), and will be separated by ten degrees to provide a 40 degree field of view.

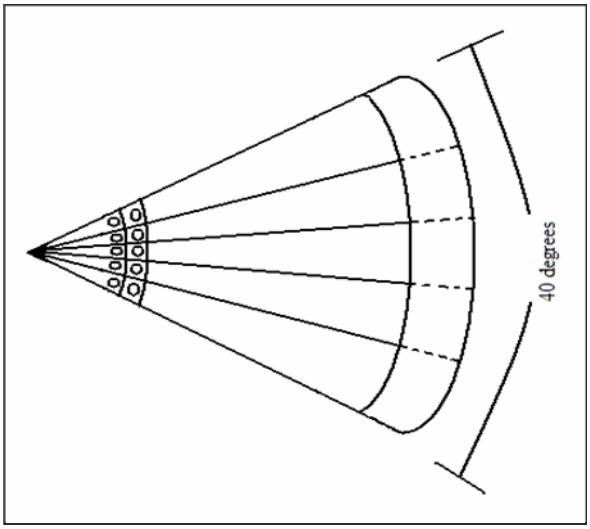

Figure 3.1.1: Photometer Housing Array

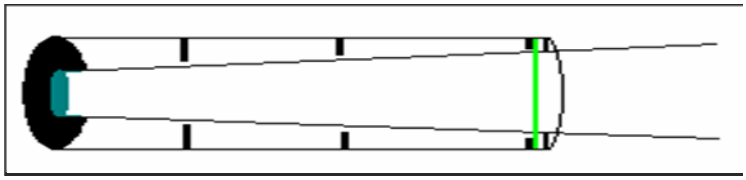

Figure 3.1.2: Photometer Channel Tube

3.2 PAST FLIGHTS

The first rocket-borne photometer to measure NLC properties in the mesosphere was prepared by Georg Witt, Ph.D. (Stockholm University) 1967 in Meteorology, with thesis: "On the Physical Properties of Mesospheric Aerosol Distributions." His first flight in 1969 found distinct NLC scattering layers, and determined radiances for effective wavelengths of 366 and 534 nm [Witt et al, 1971]. He also found a high degree of linear polarization, and under the assumption that the particles were spherical with refractive index 1.33, he concluded that the upper limit of particle radii was 0.2 μm. Seven years later Dr. Witt was involved with a second flight. This time however, he chose effective

wavelengths of 256 and 536 nm, and concluded an upper limit of particle radii at 0.05 μm [Witt et al, 1978].

3.3 GENERAL CIRCUIT FUNCTIONALITY

The intensity of the scattered radiation will be converted to a proportional voltage via an integrated photodiode/amplifier package. After this signal is buffered, it will be compared to three reference voltages. If the input signal is less than the first reference voltage, it will be passed through to the lower channel for scaling; if the input signal is between the second and third reference voltages, it will be pass through the upper channel for scaling. Such scaling will provide the flight computer two 0 - 5 V voltages ranges for analog to digital conversion (see Figure 3.3.1).

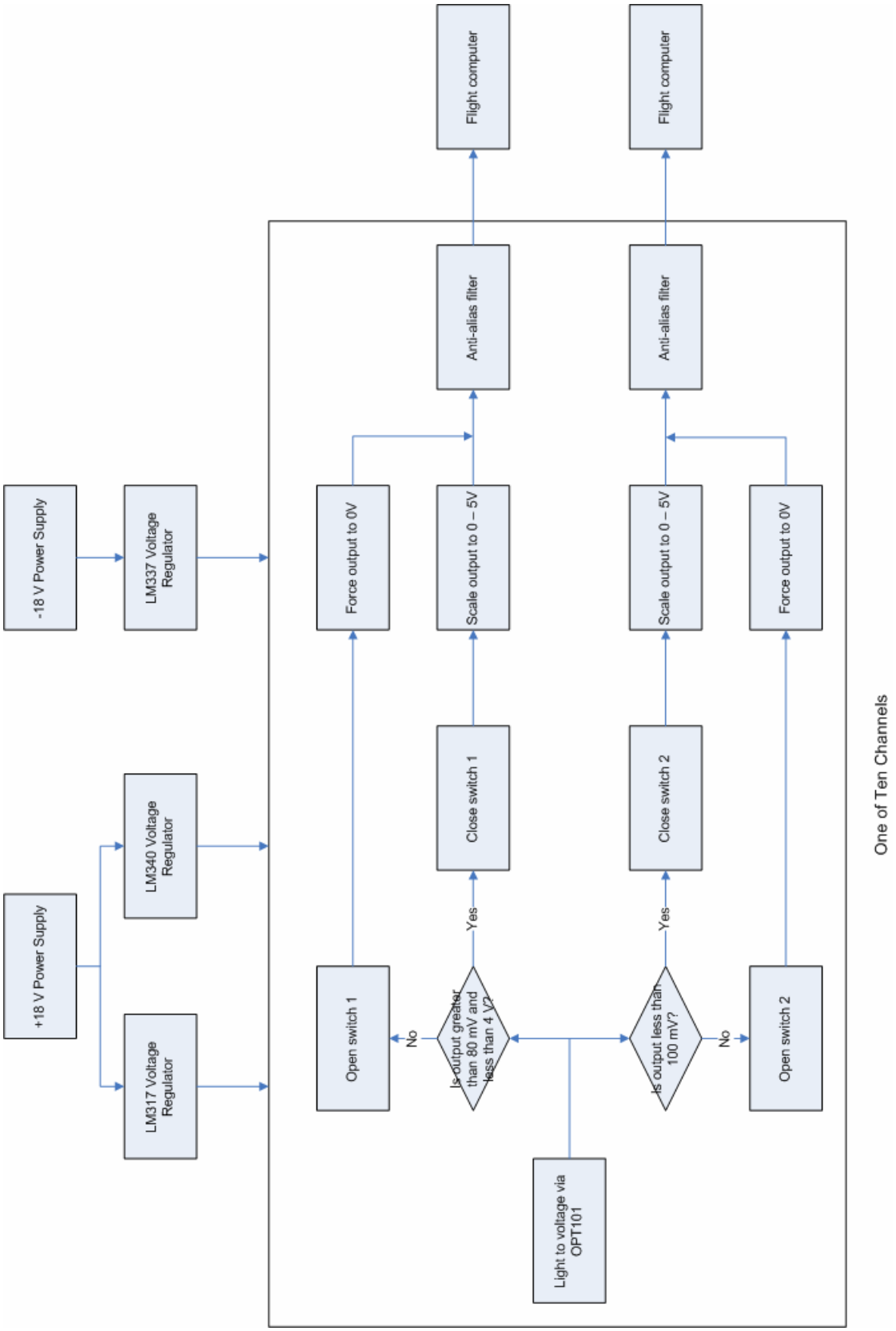

Figure 3.3.1: Block Diagram of Photometer Electronics

3.4 DETAILED CIRCUIT DESCRIPTION

The photometer's electronics begin with the OPT101, whose power supply is accompanied by a 0.1 μF bypass capacitor and a 10 MΩ feedback resistor to increase responsivity. The high precision OPA177 then buffers the output that follows from the OPT101. The buffered output is next compared to three reference voltages, achieved by voltage division of a regulated source; the output to the first comparator goes high when the OPT101's output is in between an upper range, and the output to the second comparator goes high when the OPT101's output is in a lower range. In effect, the two LM339 comparators act as digital inputs to the MAX4622 switch that follows. With switch one high, it closes and passes the OPT101's buffered output to the following OPA177 for signal scaling; with switch one low, the voltage at pin 4, achieved by voltage division of a regulated source, is instead passed to force a 0 V output to the OPA177. Similarly, with switch two high, it closes and passes the OPT101's buffered output to the following OPA177 for signal scaling; with switch two low, the grounded voltage at pin 5 is instead passed to force a 0 V output to the OPA177. The first OPA177 for signal scaling first subtracts the original reference voltage and scales the voltage for ADC, as this channel represents the upper voltage range. The second OPA177 just scales the voltage for ADC, as this channel represents the lower voltage range. Both channels are then anti-alias filtered via MAX7480, an 8-pole Butterworth filter; the corner frequency is controlled by the LM339, which is configured to act as a clock (see Figure 3.4.1).

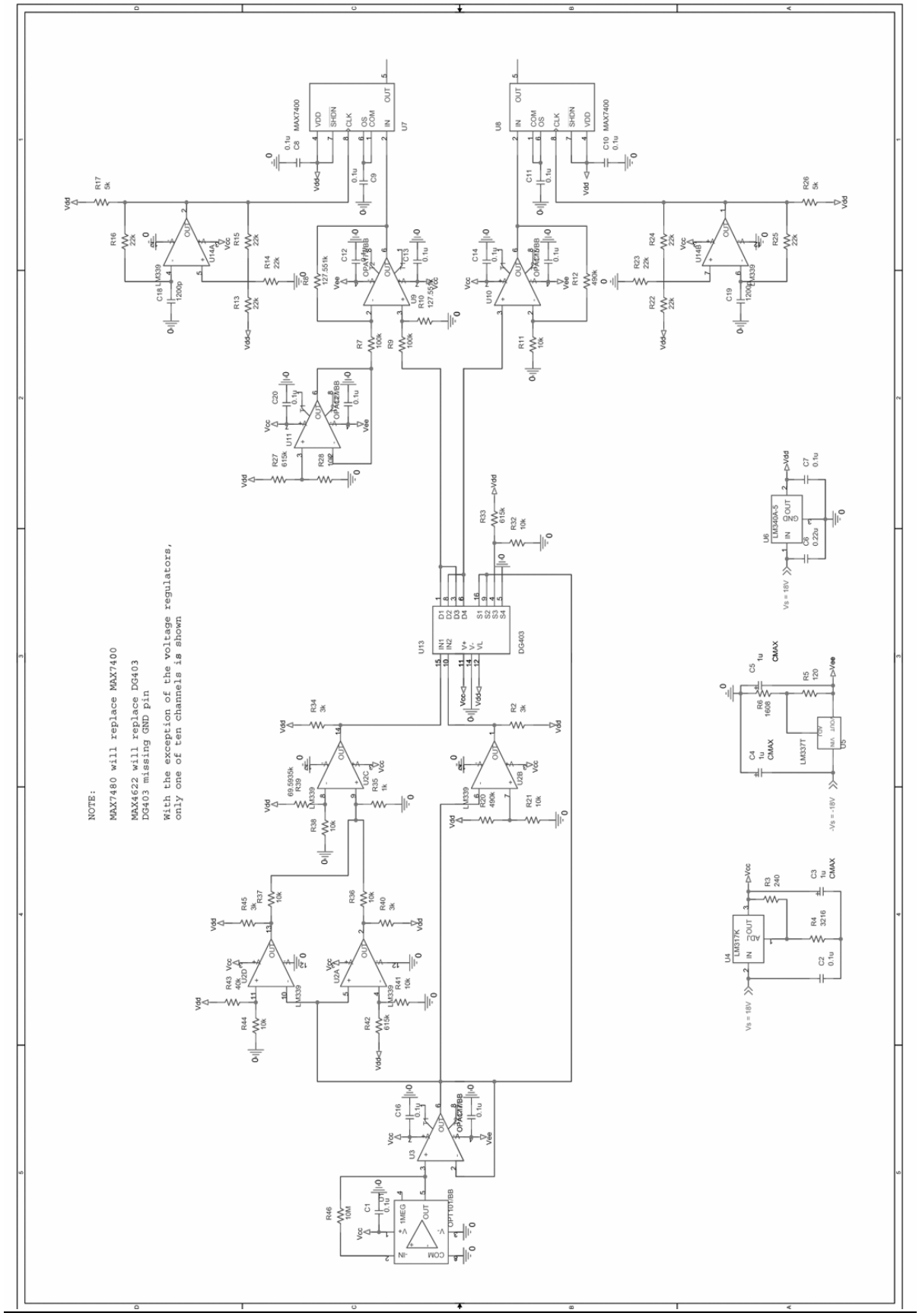

Figure 3.4.1: Complete Photometer Schematic

3.5 LAB TESTS

Photodiode/Amplifier IC - OPT101

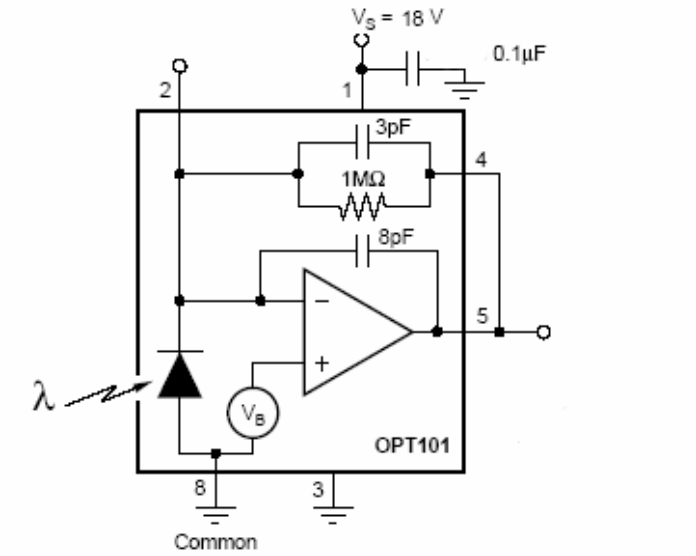

Figure 3.5.1: OPT101 circuit connection

Figure 3.5.1 shows the inner circuitry of the OPT101, a photodiode/amplifier IC. The 5° viewing angle to the photodiode was achieved using a cylindrical test tube with a length of 13.74 cm, and a diameter of 1.2 cm. Table 3.5.1 shows several OPT101 outputs from measuring different sources.

Description	With tube or without?	Output (V)
Ambient light (in Lab)	With	0.15
Ambient light (in Lab)	Without	5.34
Blue sky	With	1.30
Blue sky	Without	17.20*
Clouds in front of sun	With	3.50
Clouds in front of sun	Without	17.20*

Table 3.5.1: OPT101 output
***Output saturated**

To determine the OPT101's linearity over a large range of intensities, three Wratten filters were placed at the end of the test tube. Wratten filters lessen light intensity according to the type of filter placed in front of the source. The following equation shows how the expected output results:

$$\text{Filtered Value} = \text{Original Value} * \frac{1}{10^{FilterType}}$$

For example, a type 0.3 Wratten filter would lessen the intensity by a factor of $\frac{1}{10^{0.3}}$, or $\frac{1}{2}$, a type 1 Wratten filter would lessen the intensity by a factor of $\frac{1}{10}$, a type 2 Wratten filter would lessen the intensity by a factor of $\frac{1}{100}$, etc. Table 3.5.2 shows the results from the Wratten filter test.

Filter Type	Output (V)	Expected Output (V)	% Error
None	2.45	n/a	n/a
0.3	1.20	1.22	1.64
1	0.242	0.245	1.22
2	0.0241	0.0245	1.63

Table 3.5.2: Wratten filter output test

Signal Comparator - LM339

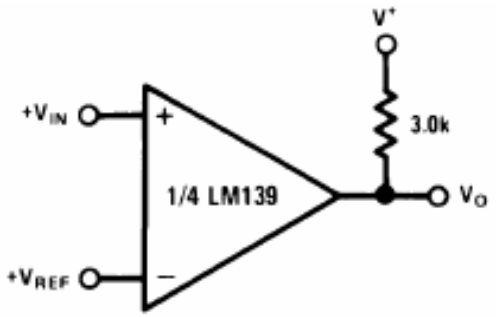

Figure 3.5.2: LM339 as basic comparator

Figure 3.5.2 shows the LM339 configured as a basic comparator. It is used as a digital input to the analog switches. Table 3.5.3 shows the comparator's output for two input and reference voltage combinations.

V_{in} (V)	V_{ref} (V)	V_o (V)
18.016	4.967	18.016
4.967	18.016	0.16151

Table 3.5.3: LM339 comparator output

Filter Clock - LM339

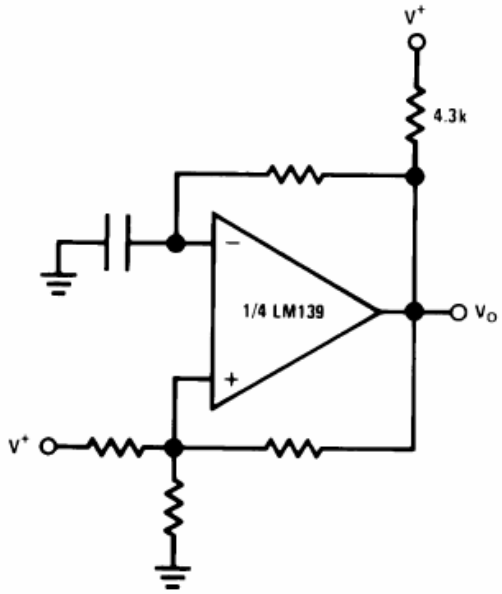

Figure 3.5.3: LM339 squarewave oscillator

Figure 3.5.3 shows the LM339 configured as a squarewave oscillator to be used as a clock to the MAX7480 Butterworth anti-aliasing filter. SPIRIT's flight computer required a -3db corner frequency of 252 Hz. The MAX7480 datasheet specifies that

$$f_{corner} = \frac{f_{clk}}{100},$$

so a clock frequency of 25.2 KHz would expect to provide the desired results; however, lab tests showed better results using a clock frequency of 24.4 KHz. Table 3.5.4 shows the values used to configure the LM339 as a clock.

R (kΩ)	C (pf)	V_o (V_{pp})	f_o (kHz)
22	1200	16.4	24.4

Table 3.5.4: LM339 squarewave oscillator output as filter clock

Signal Routing - LM339

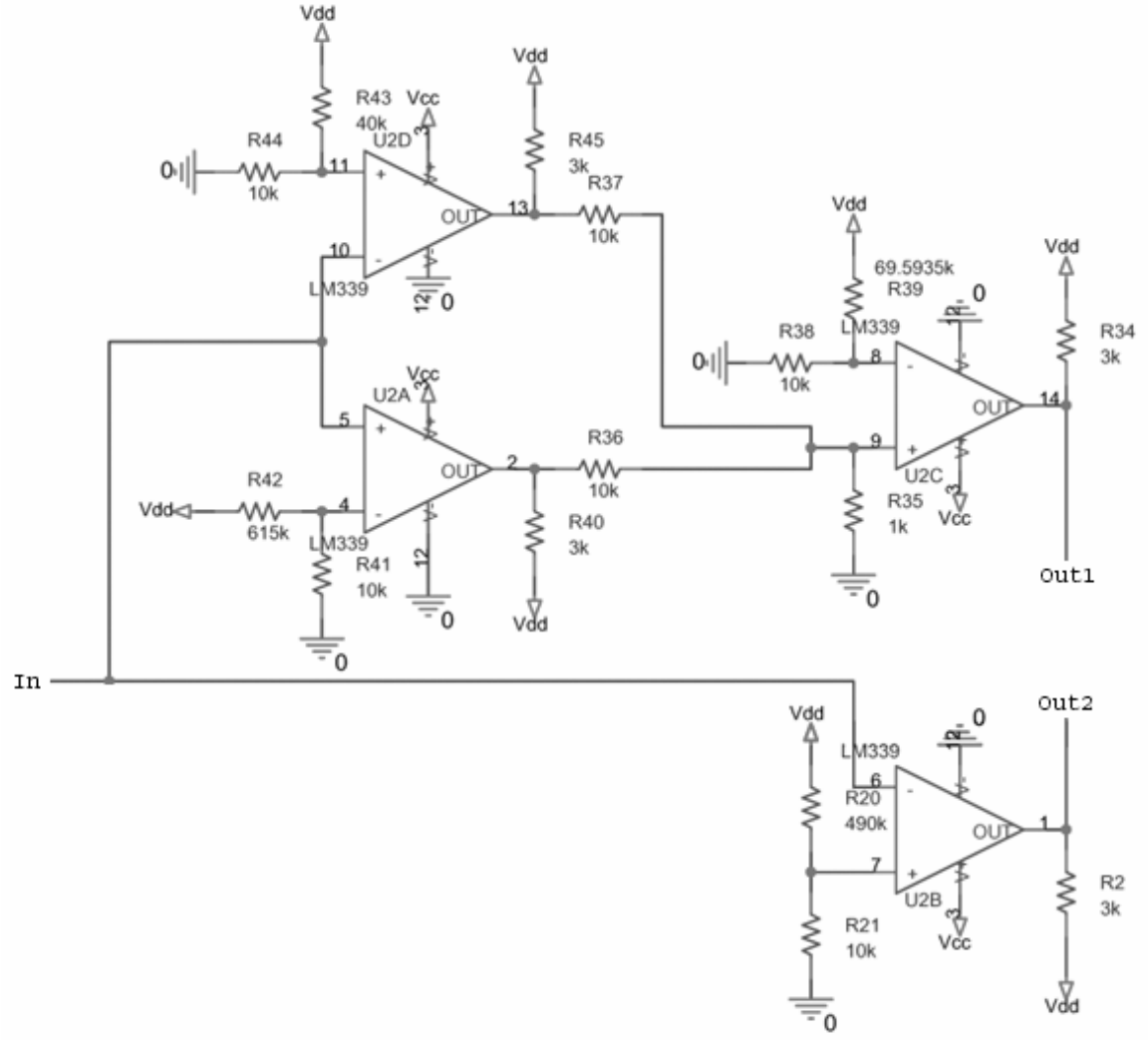

Figure 3.5.4: LM339 as comparator and digital input to switch

Figure 3.5.4 shows the LM339 configured as both a comparator and a digital input to the analog switch that follows. U2 A, C and D route the upper voltage range, 0.08 - 4 V, and U2 B routes the lower voltage range, 0 - 0.1 V. The reference voltages to which the signals are compared are provided by voltage division of a 5 V regulated source, V_{dd}. 4 V is seen at pin 11, 0.08 V is seen at pin 4, and 0.1 V is seen at pin 7. When the input, which comes from the OPT101's buffered output, is less than 0.1 V, Out2 goes high. When the input is between 0.08 and 4 V, Out1 goes high; otherwise the outputs are low. Table 3.5.5 shows the results for several inputs.

In (V)	Out1 (V)	Out2 (V)
0.02185	0.075	4.9993
0.09059	5.000	5.000
1.00358	4.9997	0.07255
3.002	4.9997	0.07257
5.0037	0.0764	0.07609

Table 3.5.5: LM339 digital input to switch output

Scaling Amplifiers - OPA177

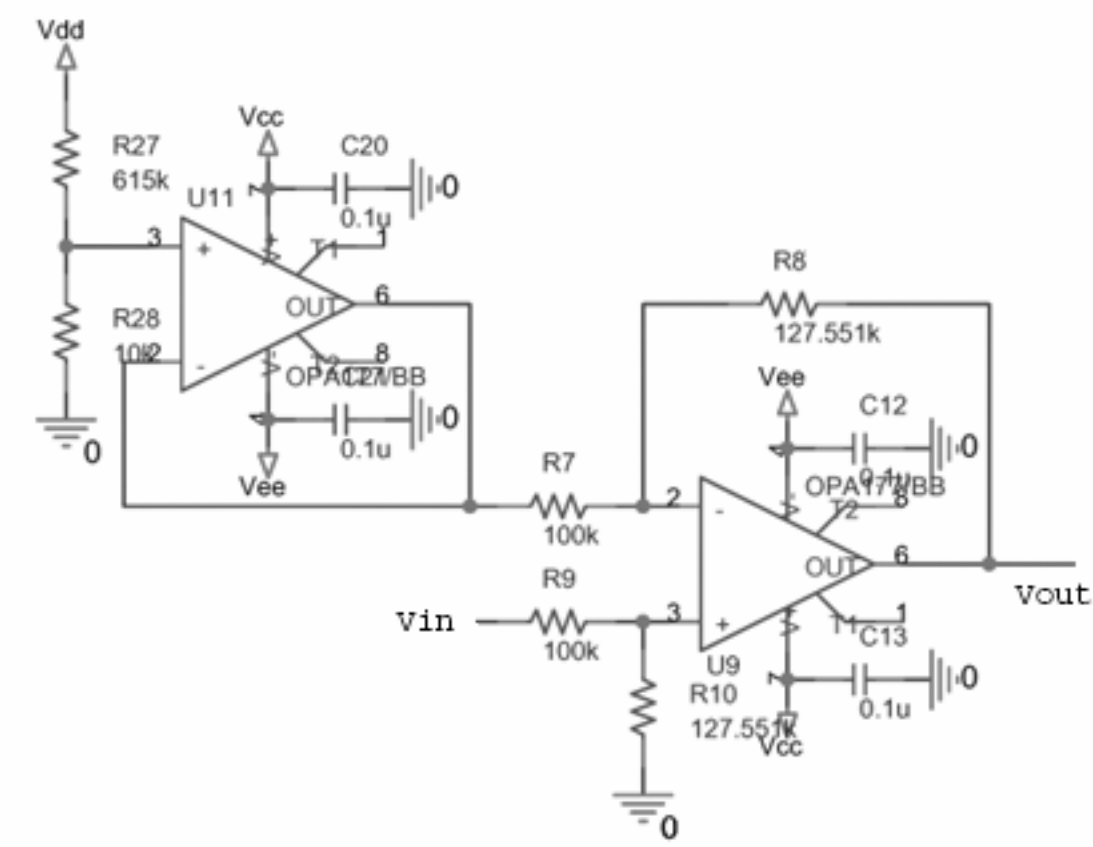

Figure 3.5.5: OPA177 difference amplifier

Figure 3.5.5 shows the high-precision OPA177 configured as a scaling difference amplifier. V_{in}, as the upper voltage channel, will be in the range, 0.08 - 4 V; this range needs to be scaled to 0 - 5 V for ADC. 0.08 V is subtracted from V_{in} using the OPA177 as a difference amplifier with the buffered reference voltage at U11 pin 6, a voltage division of 5 V, or V_{dd}, at U2 pin 3. The voltage is then scaled by the feedback and input resistors, R7 through R10, allowing V_{out} to emerge as

$$V_{out} = (1.28)(V_{in} - 0.08\ V)$$

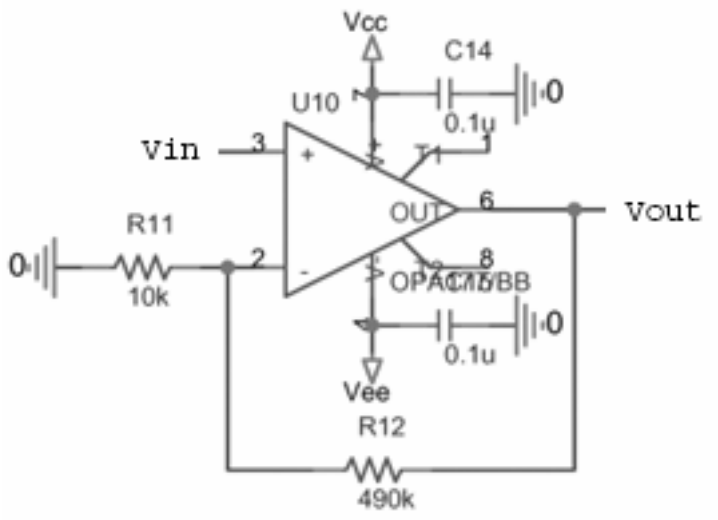

Figure 3.5.6: OPA177 non-inverting amplifier

Figure 3.5.6 shows the OPA177 configured as a non-inverting amplifier. V_{in}, as the lower voltage channel, will be in the range, 0 - 0.1 V; this range needs to be scaled to 0 - 5 V for ADC. The voltage is scaled by the feedback resistors, R11 and R12, allowing V_{out} to emerge as

$$V_{out} = (50)(V_{in})$$

Butterworth Anti-Aliasing Filter - MAX7480

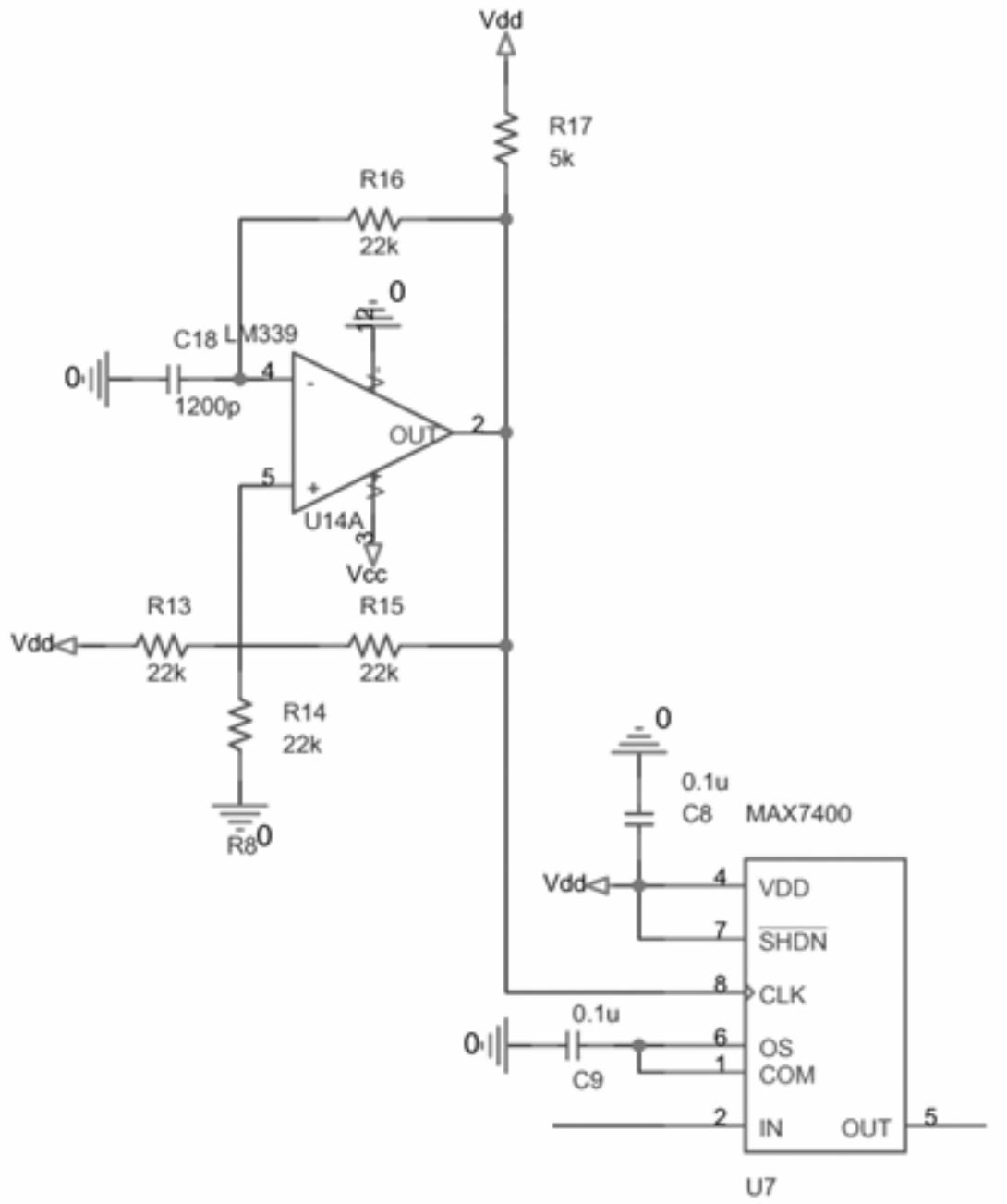

Figure 3.5.7: MAX7480 Butterworth anti-aliasing filter

Figure 3.5.7 shows the MAX7480 configured as an anti-aliasing filter, using the clock from Figure 3.5.3. The connections are typical, from the MAX7480 datasheet. Table 3.5.6 shows results for the signal attenuation.

V_{in} (V_{pp})	f_{in} (Hz)	V_{out} (V_{pp})	Attenuation (dB)
2.10	252	1.34	-2.65
2.13	780	0.031	-28

Table 3.5.6: MAX7480 Butterworth anti-aliasing filter output

Analog Switch - MAX4622

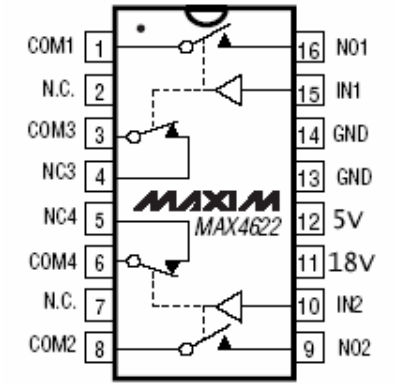

Figure 3.5.8: MAX4622 analog switch

Figure 3.5.8 shows the MAX4622, a single-pole/double-throw analog switch. When the digital input, IN (from the LM339 comparators), goes high, the normally open pin, NO, will couple to the output, COM. When the digital input goes low, the normally open pin will remain open, and the normally closed pin, NC, will stay coupled to the output. Tying both the normally open and normally closed pins together allows either voltage, NO or NC, to be seen at the same node, at different times, depending on the input.

NO1 (V)	NC3 (V)	IN1 (V)	COM1/3 together (V),(mA w/ R_L = 1kΩ)
18.226	2.9994	0	2.9994, 3.0120
18.226	2.9994	5	18.226, 18.472
0.000003	2.9994	0	2.9994, 3.0120
0.000003	2.9994	5	0.000006, 0

Table 3.5.7: MAX4622 analog switch output

Table 3.5.7 shows several switch outputs with different NO and NC voltages and different digital inputs.

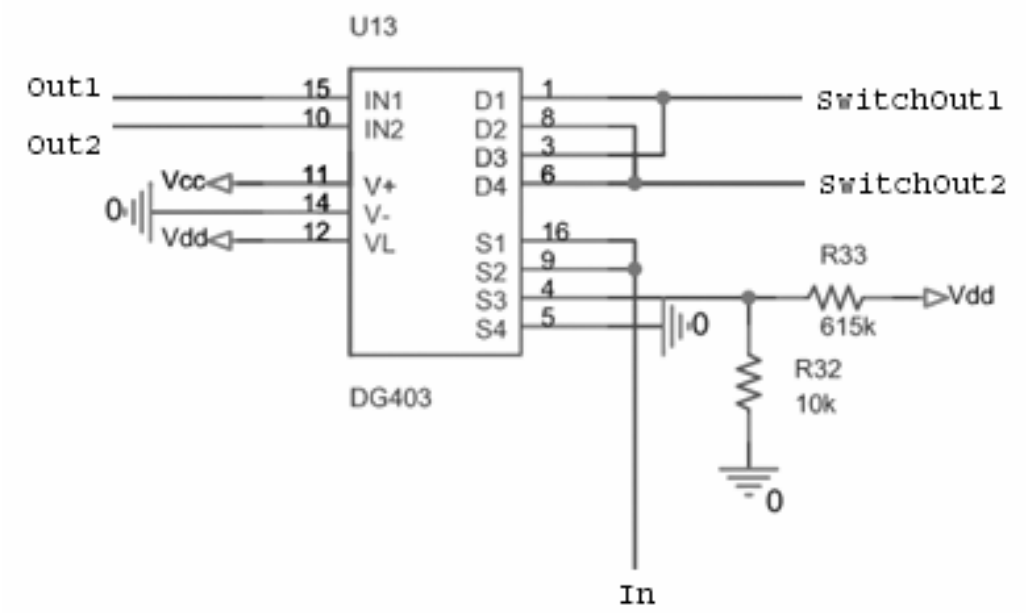

Figure 3.5.9: MAX4622 analog switch (with LM339 as digital inputs)
***Out1, Out2 from Figure 3.5.4**

Figure 3.5.9 shows how the MAX4622 SPDT analog switch will be used in the photometer. When Out1, from the comparators of Figure 3.5.4 goes high, the photodiode/amplifier output is in the upper range, 0.08 - 4 V, and will couple to SwitchOut1 which follows to the scaling difference amplifier of Figure 3.5.5; if Out1 is low, a 0.08 V reference at pin 4 will be coupled to SwitchOut1. When Out2 goes high,

the photodiode/amplifier output is in the lower range, 0 - 0.1 V, and will couple to SwitchOut2 which follows to the non-inverting amplifier of Figure 3.5.6; if Out2 is low, SwitchOut2 will couple to ground, pin 5. Table 3.5.8 shows the switch output voltages for inputs that are expected photodiode/amplifier outputs.

In (V)	SwitchOut1 (V)	SwitchOut2 (V)
0.01964	0.081110	0.01974
0.094027	0.094004	0.094010
0.19961	0.1996	0.000907
1.00160	1.00157	0.000259
3.0019	3.0019	0.000284
5.0032	0.079935	0.000482

Table 3.5.8: MAX4622 analog switch (with LM339 as digital inputs) output

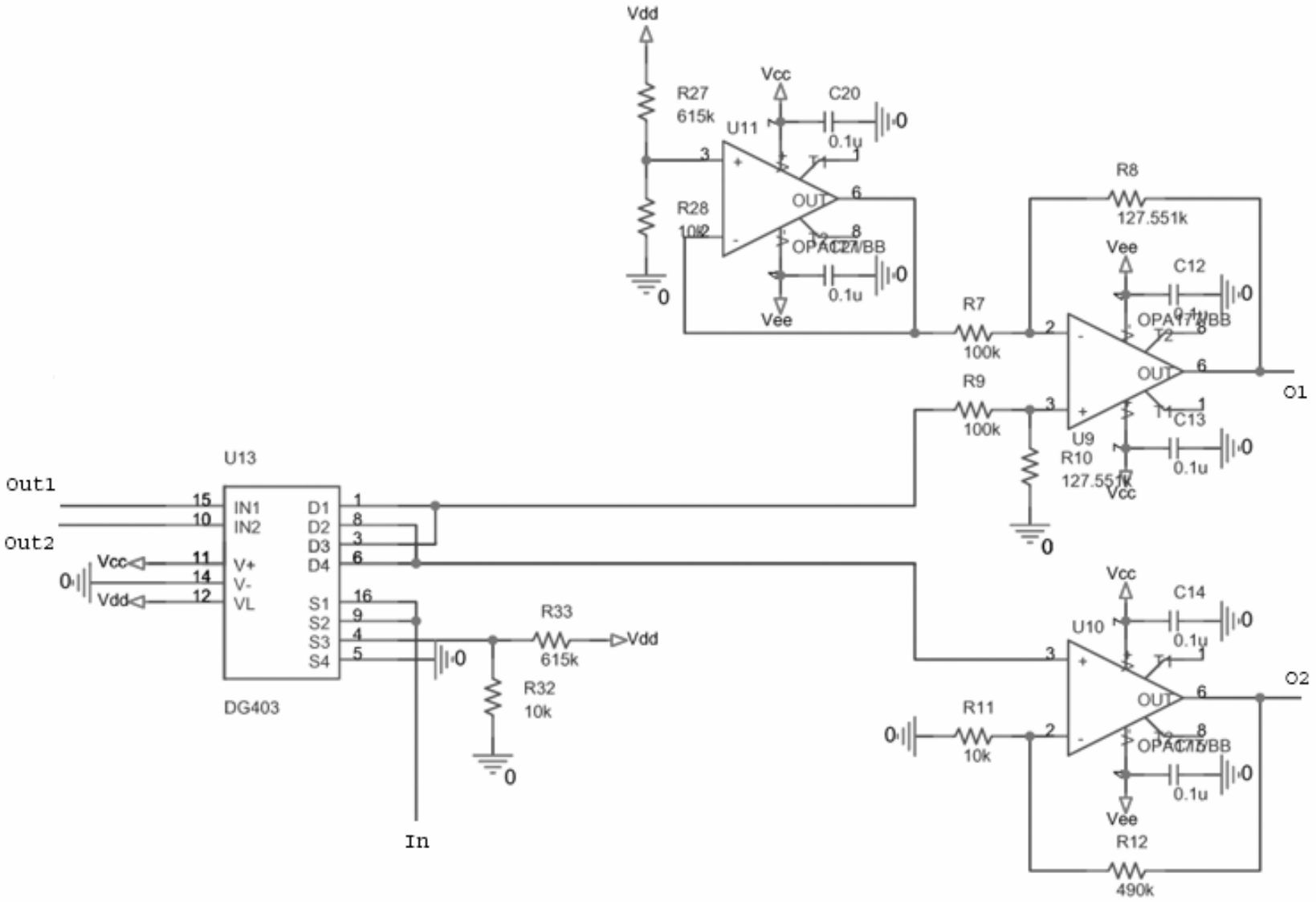

Figure 3.5.10: MAX4622 analog switch (with LM339 as digital inputs) to scaling OPA177 amplifiers
***Out1, Out2 from Figure 3.5.4**

Figure 3.5.10 shows the analog switch of Figure 3.5.9 and the scaling amplifiers of 3.5.5/6 together as the last stage of the photometer, before the anti-aliasing filters. Expected outputs are

$$O1 = (1.28)(V_{in} - 0.08\ V)$$

$$O2 = (50)(V_{in})$$

Table 3.5.9 shows experimental results of this last stage.

In (V)	O1 (V)	Expected O1 (V)	% Error	O2 (V)	Expected O2 (V)	% Error
0.019678	-	-	-	0.81316	0.9839	17.4
0.060	-	-	-	2.7323	3.000	8.92
0.200	0.15192	0.1536	1.09	-	-	-
1.00089	1.15120	1.179	2.36	-	-	-
3.0019	3.6468	3.7400	2.49	-	-	-

Table 3.5.9: MAX4622 analog switch (with LM339 as digital inputs) to scaling OPA177 amps output

3.6 DATA ANALYSIS

Each of the photometer's ten channels will have two analog outputs, 0 - 5V, both representing different voltage outputs from the OPT101. The first channel represents the upper voltage range, 0.08 - 4.00V; the second channel represents the lower voltage range, 0 - 0.1V.

The scaling amplifiers provide the conversion from the two ranges to the acceptable 0 - 5 V range for ADC. The first channel's scaling equation is

$$V_{out} = (1.28)(V_{in} - 0.08\ V),$$

so to find the original photodiode/amplifier output voltage, the equation's inverse is determined as

$$V_{in} = \frac{V_{out}}{1.28} + 0.08.$$

The second channel's scaling equation is

$$V_{out} = (50)(V_{in}),$$

so to find the original photodiode/amplifier output voltage, the equation's inverse is determined as

$$V_{in} = \frac{V_{out}}{50}.$$

The original photodiode/amplifier output voltage is directly proportional to the solar radiation incident upon it. Figure 3.6.1 shows the relationship between intensity and output voltage for specific incident wavelengths.

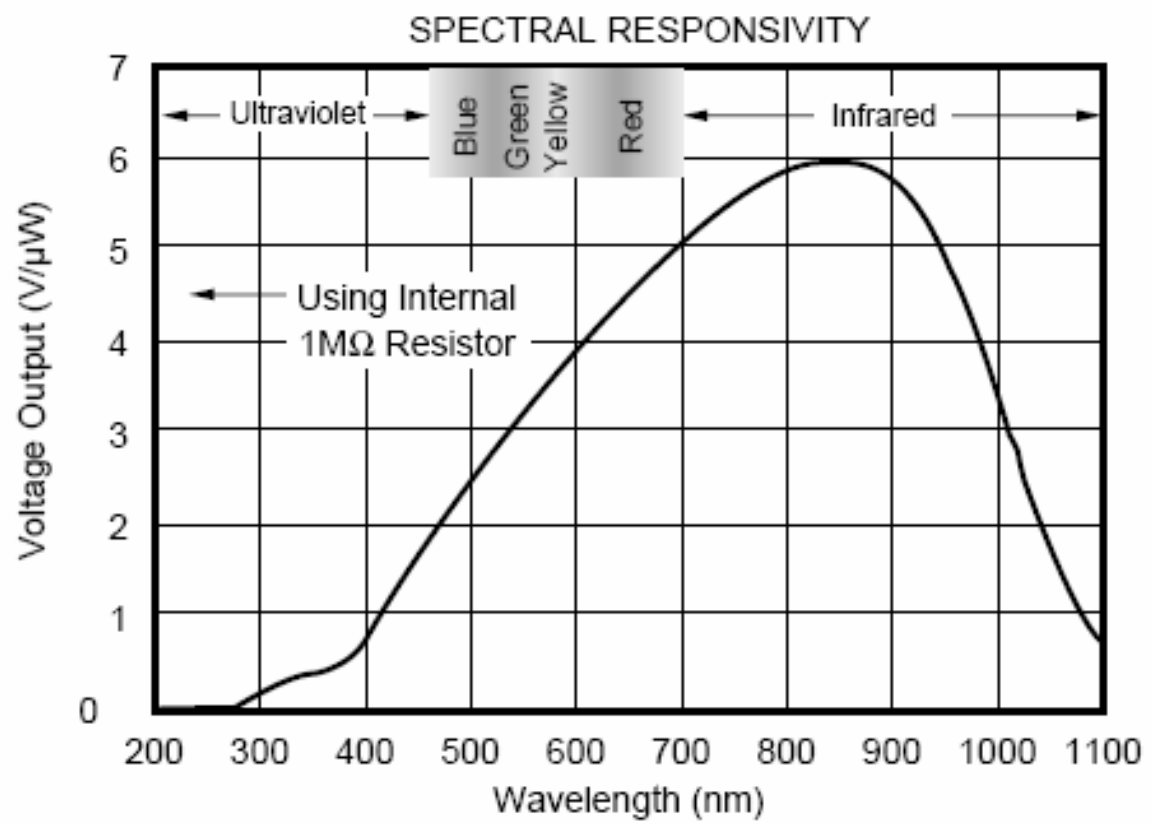

Figure 3.6.1: Spectral Responsivity of OPT101

For example, suppose a 550 nm passband filter is used on one channel of the photometer. From Figure 3.6.1, a 550 nm wavelength has a spectral responsivity of about 3 V/μW; the solar radiation intensity can thus be determined by dividing the photodiode/amplifier output voltage by this responsivity.

3.7 DATA CONCLUSION

For every spin cycle of the SPIRIT rocket, solar radiation intensity at all scatter angles will be collected by the flight computer. The photometer accompanies a sun sensor for determining such a scatter angle between the sun and the rocket's spin axis. By noting the time between a sun pulse and a photometer sample, solar radiation intensity data can be associated with a particular scatter angle. The intensities can then be plotted on a polar plot similar to those mentioned in the MATLAB examples of section 2.2. Comparing the experimental scatter plots and thus the forward to back scatter ratios to that predicted by the Mie Scattering theory computer model, particle size and distribution can be determined.

4 CONCLUSION

SPIRIT's optics team has interest in investigating the properties of Noctilucent clouds present in the mesosphere. NLC properties will lend a better understanding of the global atmospheric changes caused by pollutants present in the atmosphere and the global energy balance.

The rocket-borne photometer will measure NLC solar radiation scatter intensities. The data gathered will be compared to that theorized by a Mie theory computer model. Conclusions can thus be drawn when similarities emerge between experiment and theory, and particle size and distribution information can be obtained.

5 BIBLIOGRAPHY

"A Dynamic Model of the Mesosphere and Lower Thermosphere," T.J. Keneshea, S.P. Zimmerman and C.R. Philbrick, Planet. Space Sci., 27:385-401, 1979.

"Mie theory." Wikipedia. Oct. 2005 <http://en.wikipedia.org/wiki/Mie_scattering>.

“Noctilucent Clouds,” M. Gadsden, W. Schröder, Physics and Chemistry in Space Planetology:1-6,46-50,58-61, 1989

“Results from Two Scattered Light Photometers on Board an AFCRL Noctilucent Cloud Particle Collecting Payload,” G. Witt and N. Wilhelm, Report AP9:4-12, University of Stockholm, 1978.

"Rocket Measurements of Mesospheric and Lower Thermospheric Composition," C.R. Philbrick, G.A. Faucher and E. Trzcinski, Space Res. XIII:255-260, Akademie-Verlag, 1973.

“Sounding Rocket Experiment for the Investigation of High-Latitude Summer Atmospheric Conditions Between 60 and 110 Km,” G. Witt, N. Wilhelm, J. Stegman, A.P. Williams, B. Holback, E. Llewellyn and A. Pederson, Report AP7:1-3, University of Stockholm, 1971.

"Temperature Measurements during the CAMP Program," C.R. Philbrick, J. Barnett, R. Gerndt, D. Offermann, W.R. Pendleton, Jr., P. Schlyter, J.F. Schmidlin, and G. Witt, Adv. Space Res., 4:153-156, 1984.

"What are NLC?" Martin, G.J., North East Noctilucent Cloud Observers Group. Mar. 2005 <http://freespace.virgin.net/eclipsing.binary/whatarenlc.html>.

ACADEMIC VITA

EDUCATION:

The Pennsylvania State University — University Park, PA
B.S. Electrical Engineering — December 2005

Thesis, *The Design and Testing of a Rocket-Borne NLC Photometer*
Adviser, Dr. C.Russell Philbrick

TECHNICAL EXPERIENCE:

Honeywell International — Ft. Washington, PA
Control Systems Test Engineer — May 2005 - Present

- Tested and calibrated analog I/O modules.
- Maintained and serviced high-capacity, performance testbed.
- Built and configured process control strategies.
- Configured and upgraded controllers and I/O modules.
- Performed system benchmark tests.

Carl Bro Group Ltd — London, England
Technical Writer — Summer 2004

- Researched the newly developed TransXChange, an XML-based UK national data standard for the interchange of bus route and timetable information.
- Worked alongside senior consultant to design a testing scheme for TransXChange.
- Created test scenarios for the said testing scheme, based on examples provided by the UK Department of Transport, and partner Kizoom Ltd.
- Drew test-specification document for client usage.

HONORS/AWARDS:

- Schreyer Honors College
  - Membership based upon academic record and nomination from the Electrical Engineering Department.
- Dean's List – 2001 through 2005
- Frank Gabron Scholarship in Electrical Engineering – 2001 through 2005
- President's Freshman Award
  - Awarded to Freshman with GPA of 4.0.